Robust Epoxy Resins with Autonomous Visualization of Damaging-Healing and Green Closed-Loop Recycling

Xuewei Jiao, Yaning Ma, Zihan Zhao, Liang Gao, Baoyan Zhang, Jigang Yang, Min-Hui Li, Jun Hu

Robust Epoxy Resins with Autonomous Visualization of Damaging-Healing and Green Closed-Loop Recycling

*Xuewei Jiao, Yaning Ma, Zihan Zhao, Liang Gao, Baoyan Zhang, Jigang Yang, Min-Hui Li and Jun Hu**

X. Jiao, Y. Ma, Z. Zhao, J. Yang, J. Hu
Beijing Advanced Innovation Center for Soft Matter Science and Engineering, Beijing University of Chemical Technology, North Third Ring Road 15, Chaoyang District, Beijing 100029, China
E-mail: jhu@mail.buct.edu.cn

L. Gao, B. Zhang
Department of Resin & Prepreg, AVIC Manufacturing Technology Institute Composite Technology Center, Shijun Road 1, Shunyi District, Beijing 101300, China

M.-H. Li
Chimie ParisTech, PSL University, CNRS, Institut de Recherche de Chimie Paris, 11 rue Pierre et Marie Curie, Paris 75005, France

Keywords: epoxy resin, high performance, disulfide bond, ester bond, closed-loop recycling

Epoxy resins-based engineering plastics are indispensable in the global economy, but they have created a serious waste crisis caused by their chemical cross-linked networks. To solve this problem, current strategies often require the assistance of catalysts or solvents at the expense of thermal and mechanical performance. In this work, a high-performance epoxy resin featuring dynamic ester and disulfide bonds (TDS) is reported, which exhibits higher thermal and mechanical properties than common engineering plastics, i.e. tensile strength and modulus

of 66.6 MPa and 2.63 GPa, flexural strength and modulus of 103.2 MPa and 3.52 GPa, and T_g of 133°C. Moreover, the reversible transformation between aromatic disulfide bonds and thiyl radicals endows TDS epoxy resin with autonomous visualization of damage and healing. In addition, the harmonious interplay between disulfide and ester bonds-promoted by tertiary amine accelerated the topological network rearrangements, enabling TDS to easily reshape and weld. Specifically, TDS can be completely degraded in pure water at 200°C without any catalyst, and the degraded products could be directly re-polymerized to achieve green closed-loop recycling. This work proposes a simple and economical strategy for the development of epoxy resin-based cutting-edge engineering plastics that are both functional and sustainable.

1. Introduction

The huge consumption and reprocessing of engineering plastics are indispensable in the global economy.[1-3] As one of the main components in engineering plastics, epoxy resins are widely used in the fields such as optical machinery, rail transit, aerospace, etc. due to their good mechanical property, dimensional stability, and chemical resistance.[4-6] Nevertheless, similar to other thermosetting polymers, they have limited functionality and sustainability because of their chemically cross-linked networks, and their continuous expansion has caused a serious global plastic waste crisis.[7-9] To solve the functionality issue, strategies like physically doping the epoxy resin by fillers and chemically modifying network structures have been applied, but these strategies always inevitably sacrifice the thermal and mechanical properties.[10-16] On the other hand, after their service life, the current post-treatment methods are still landfilling, incineration, and pyrolysis, which cause the secondary environmental pollution.[17,18] Therefore, the development of epoxy resin-based cutting-edge engineering plastics that are both sustainable and functional remains a major challenge.

The emergence of covalent adaptive networks (CANs) offers a potential solution to the aforementioned challenge. Based on the dynamic bonds-facilitated topological network rearrangements, thermosets possessing CANs can be reprocessed and recycled akin to thermoplastics.[19-21] Compared with the external catalyst-assisted CANs, auto-catalytic CANs always give more preferable mechanical performance because of the elimination of interfacial

problems between external catalysts and networks.[22-24] As for auto-catalytic CANs featuring dynamic ester bonds, the introduction of flexible segments,[25,26] multiple active sites,[27-29] and neighboring group participation (NGP) effect[30,31] into the networks is especially useful to obtain CANs with both robust mechanical attributes and swift recombination capabilities. In addition, due to the low bond energy, disulfide bond often works in tandem with other dynamic bonds to construct thermally reconfigurable auto-catalytic CANs.[32-34] Notably, thiyl radicals can be produced from the cleavage of disulfide bond engendered by mechanical force, which show green luminescence before pairing into disulfides again.[35,36] Thus, the use of auto-catalytic CANs with both dynamic ester and disulfide bonds is a promising strategy to prepare sustainable and multifunctional polymer materials.

In this work, we have synthesized this kind of high-performance epoxy resins featuring dynamic ester and disulfide bonds-based CANs, made of commercial epoxy (TDE-85), 4,4'-dithio-diphenylamine (4-DTDA) and sebacic acid (SA) (**Scheme 1**a). Guaranteed by the rigid skeleton in 4-DTDA, the resulting TDE-85/4-DTDA/SA (TDS) exhibited superior fracture strength (66.6 MPa), flexural strength (103.2 MPa), and high glass transition temperature (133°C), which was comparable with commercial resins. The reversible transformation between aromatic disulfide bonds and thiyl radicals endowed TDS with mechanochromic property for autonomous visualization of resin damage and healing (Scheme 1b). Moreover, the harmonious interplay between disulfide and ester bonds-promoted by tertiary amine accelerated the topological network rearrangements (Scheme 1c), which make TDS to easily reshape, weld, degrade, and recycle. Specifically, the complete degradation of TDS was carried out in pure water within 10 h, and the degradation products could be reused to produce again TDS without further separation and modification (Scheme 1d). This work proposed a promising strategy to prepare functional and eco-friendly epoxy materials.

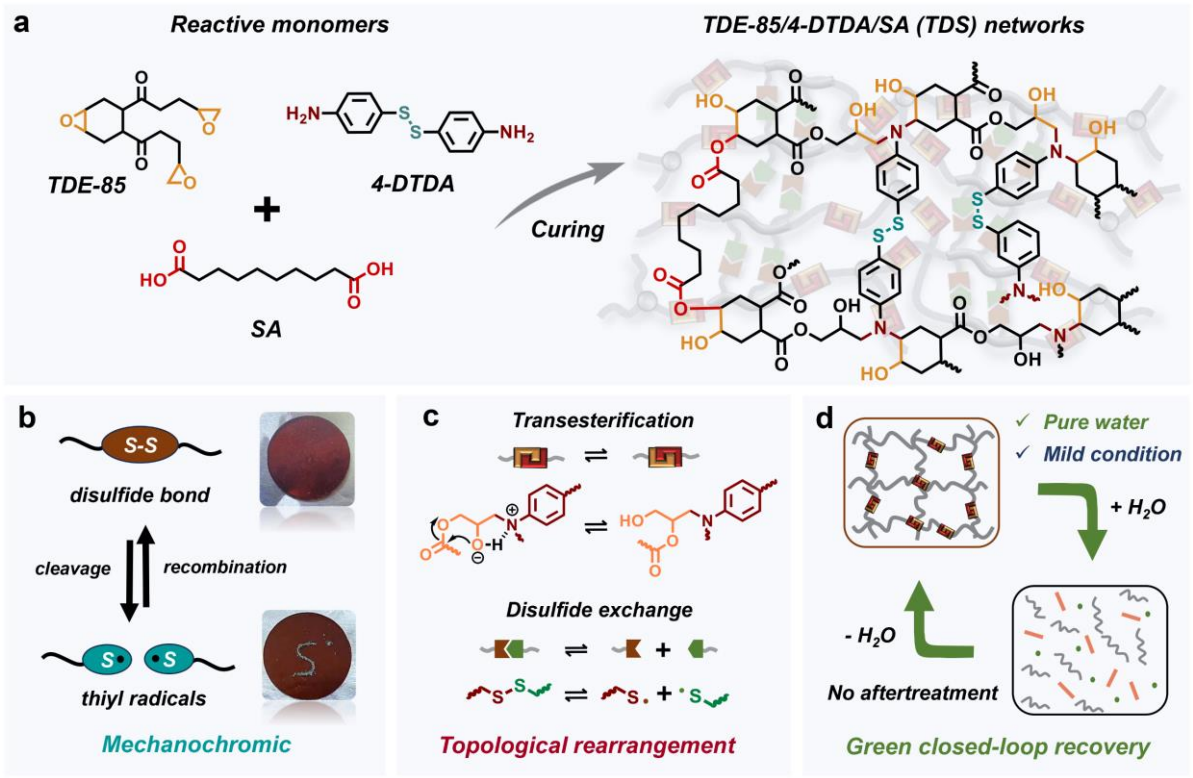

Scheme 1. Design concept of TDE-85/4-DTDA/SA (TDS) networks featuring dynamic ester and disulfide bonds. a) Chemical structures of reactive monomers and the cross-linked networks. b) Damage and healing sensing functions promoted by the reversible transformation between disulfide bonds and thiyl radicals. c) Topological network rearrangements facilitated by the harmonious interplay between disulfide and ester bonds-promoted by tertiary amine. d) Schematic illustration of the green closed-loop recovery.

2. Results and discussion

2.1 Synthesis, thermal, and mechanical properties

The cross-linked networks of TDS were prepared by curing glycidyl ester (TDE-85) with 4,4'-dithiodianiline (4-DTDA) and sebacic acid (SA) at different molar ratios (R), where R of -COOH/-NH group was set as 7/3, 6/4, 5/5, 4/6, and 3/7, while maintaining an equal epoxy content (Table S1, Supporting Information). Accordingly, the cured networks were denoted as TDS-V1, TDS-V2, TDS-V3, TDS-V4, and TDS-V5, respectively. Differential scanning calorimetry (DSC) showed that the curing of carboxylic acid/epoxy and amine/epoxy group occurred around 110°C and 140°C, respectively (Figure S1, Supporting Information). For ensuring the complete curing and avoiding degradation of raw materials, the curing program

was designed to be pre-cured at 90°C/30 min followed by "120°C/1 h + 150°C/2 h + 180°C/2 h". The resulting TDS had good formability, transparency, and smooth surface (**Figure 1**a), and the cross-linked networks were confirmed by DSC and fourier-transform infrared (FTIR) spectra. No significant residual heat peak was observed on DSC curves for TDS networks (Figure S2, Supporting Information). After curing the peaks of epoxy at 905/853 cm^{-1}, carboxyl acid at 1710 cm^{-1}, and aromatic amine at 3417/3331/1624 cm^{-1} disappeared in FTIR spectra, accompanied with a generation of hydroxyl peak at 3400 cm^{-1} (Figure 1b and S3, Supporting Information), which indicated that the curing reaction was completed. Moreover, the results of gel content showed that TDS only swelled but was almost insoluble in organic solvent with a gel content of over >90% and a low swelling ratio (Table S2, Supporting Information). After immersing TDS-V4 as a representative in tetrahydrofuran (THF), methanol (MeOH), ethanol (EtOH), acetone (Act.), chloroform (TCM), toluene (PhMe), ammonia (NH_4OH), H_2O, H_2SO_4 (1 M) and HCl (1 M) at room temperature for 28 days, it remained intact (Figure 1c). All above results revealed the cross-linked networks of TDS with strong chemical resistance to organic solvents, alkaline and acidic solutions.

The thermal properties of TDS networks were firstly evaluated by dynamic mechanical analysis (DMA) with a double cantilever under a heating rate of 3°C min^{-1}. As shown in Figure 1d, TDS networks possessed the storage modulus (E') at glass platform ranged from 1.29 to 2.22 GPa, and exhibited typical thermosetting behavior with a storage modulus (E') platform above the glass transition temperature (T_g). With increasing the content of rigid chains originated from 4-DTDA, the E' at rubbery state increased from 4.5 to 29.7 MPa for TDS-V1 to TDS-V5. Accordingly, their cross-linking density (v_e) was calculated to be 521, 1099, 1991, 2292 and 2555 mol m^{-3} (**Table 1**). Because of the adjustable rigidity, TDS networks had a wide tunable T_g, which was 35, 70, 97, 133, and 163°C, respectively, for TDS-V1, TDS-V2, TDS-V3, TDS-V4 and TDS-V5. Moreover, the results of thermogravimetric analyzer (TGA) showed that the initial weight loss ($T_{d5\%}$) of TDS networks occurred at temperatures above 270°C, indicative of good thermal stability (Figure S4a, Supporting Information). And the mass loss peak in the temperature range of 270 to 300°C gradually enlarged from TDS-V1 to TDS-V5 in

thermogravimetric derivative (DTG) curve, which was attributed to the decomposition of more disulfide bonds (Figure S4b, Supporting Information).

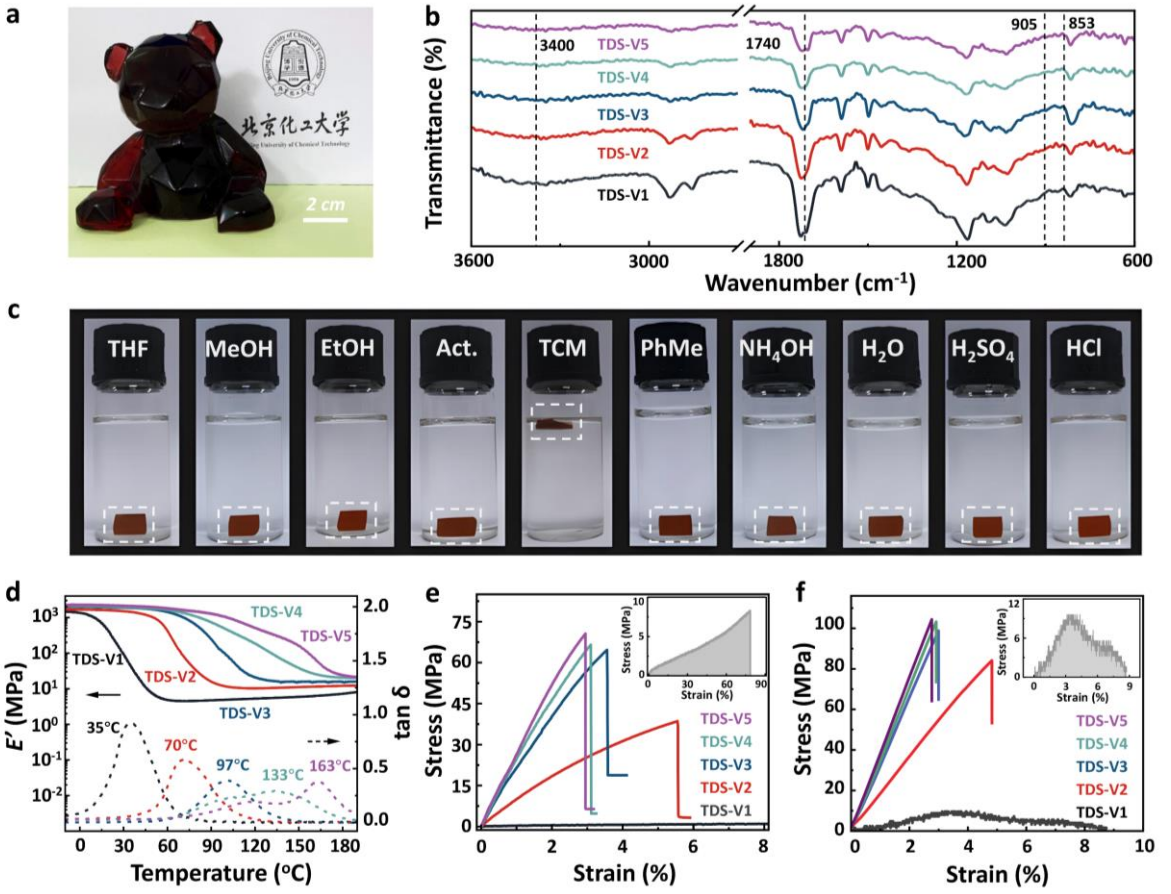

Figure 1. Synthesis, thermal, and mechanical properties. a) Digital photo of "lucky bear" made from TDS-V4 using a silicone mold. b) FTIR spectra of TDS networks in the wavenumber range from 3600-600 cm^{-1}. c) Digital photos of TDS-V4 after immersing in different solvents at room temperature for 28 days. All sample sizes are 5×5×2 mm^3. d) Storage modulus *E'* and loss angle tangent tan δ as a function of temperature from -10 to 190°C under a heating rate of 3 °C min^{-1}. e) Tensile stress-strain curves of TDS networks at a stretching rate of 2 mm min^{-1}. Local amplification curve of TDS-V1 was on the top right corner. f) Flexural stress-strain curves of TDS networks at a loading rate of 2 mm min^{-1}. Local amplification curve of TDS-V1 was on the top right corner.

The mechanical properties of TDS networks were evaluated by tensile tests. All of them exhibited rigid tensile behaviors without yield points, and their performance were adjustable, i.e. the fracture strength of 6.7, 38.6, 64.5, 66.6 and 70.6 MPa for TDS-V1, TDS-V2, TDS-V3,

TDS-V4, and TDS-V5, respectively, along with Young′s modulus of 0.01, 1.05, 2.33, 2.63, and 2.78 GPa (Figure 1e and S5, Supporting Information). Flexural tests afforded the similar trend of mechanical properties of TDS networks. As the increase of 4-DTDA content, the flexural modulus increased from 0.02 to 1.84, 3.24, 3.52, and 3.80 GPa for TDS-V1, TDS-V2, TDS-V3, TDS-V4, and TDS-V5, respectively, accompanied with the flexural strength of 9.6, 84.1, 98.8, 103.2, and 104.4 MPa (Figure 1f and S6, Supporting Information). In general, higher cross-linking density and more rigid groups are two key factors in improving the modulus or stiffness of thermosetting plastics.[37,38] The introduction of 4-DTDA led to an enhanced rigidity of the cross-linked network and a shorter distance between cross-linking points, thus resulting in a significant improvement in mechanical performance. Compared with other common commercial engineering plastics including bisphenol A diglycidyl ether/4,4'-diaminodiphenylmethane (E51-DDM), bisphenol A diglycidyl ether/primary amine (E51-D230), Hansen resin (RIMR-135/RIMH-1366), Araldite epoxy resin (®LY 1564*/Ar.5003-1*) and Makrolon polycarbonate (FR6005), our TDS-V4 and TDS-V5 had similar or even higher thermal and mechanical properties (Table S3, Supporting Information). In terms of the material cost, mechanical properties, and thermal stability, TDS-V4 was selected as a representative for the subsequent research.

Table 1 Thermal and mechanical properties of TDS networks

Sample	T_g (°C)[a]	E' (MPa)[b]	v_e (mol m^{-3})[c]	Fracture strength (MPa)[d]	Young′s modulus (GPa)[d]	Flexural strength (MPa)[e]	Flexural modulus (GPa)[e]
TDS-V1	35	4.5	521	6.7 ± 1.2	0.01 ± 0.003	9.6 ± 0.5	0.02 ± 0.01
TDS-V2	70	10.5	1099	38.6 ± 1.7	1.05 ± 0.07	84.1 ± 1.9	1.84 ± 0.26
TDS-V3	97	20.4	1991	64.5 ± 1.5	2.33 ± 0.12	98.8 ± 2.3	3.24 ± 0.17
TDS-V4	133	28.5	2292	66.6 ± 2.7	2.63 ± 0.09	103.2 ± 2.6	3.52 ± 0.21
TDS-V5	163	29.7	2555	70.6 ± 2.2	2.78 ± 0.12	104.4 ± 1.7	3.80 ± 0.29

[a]T_g value was obtained from DMA curves in Figure 1d; [b]E' at rubbery state was acquired from DMA testing at T_g + 30°C Figure 1d; [c]v_e was calculated using rubber elasticity equation of E'

= $3\nu_e RT$; [d]Fracture strength and Young's modulus were calculated from tensile stress-strain curves in Figure 1e. [e]Flexural strength and flexural modulus were calculated from flexural stress-strain curves in Figure 1f.

2.2 Dynamic network performance

The dynamic performance of TDS-V4 was firstly investigated by stress relaxation test using DMA in a tensile mode. At moderate temperatures of 180 to 220°C, TDS-V4 exhibited typical Arrhenius temperature-dependent behavior, and its modulus quickly relaxed to 1/e in a short period of time (**Figure 2**a). The relaxation time τ^*, defined as the point when the modulus relaxed to 1/e of the initial one, was 183 s at 180°C, 78 s at 200°C, and only 20 s at 220°C. This rapid dynamic bond exchange made TDS-V4 easily malleable, and its malleable temperature (T_{mall}) was determined to be 173°C by thermomechanical analysis (TMA) in three-point compression mode (Figure 2b). The corresponding displacement-temperature curve can be divided into three regions as follows: (1) the glassy state (<133^{o}C, below T_g), where molecular chain segments were frozen; (2) the rubber state (>133^{o}C and <173 ^{o}C, above T_g and below T_{mall}), where, when the temperature reached above T_g, molecular chain segments had strong fluidity but maintained elasticity; (3) the viscoelastic transition region (>173 ^{o}C, above T_{mall}), after which molecular chains moved and presented a viscous flow state.

The above mentioned T_{mall} was great helpful to guide the dynamic processing of TDS-V4 like welding and re-shaping. Compared to the topological freezing transition temperature (T_v) determined by extrapolation from the Arrhenius equation, T_{mall} can more accurately reflect the temperature for topological network rearrangements as it fully considered the network rigidity and chain segment motions.[12,26] As shown in Figure S7, the splines of TDS-V4 can be welded into diverse 3D structures such as knee table, cubic dice, and windmill box. To explore the welding ability of TDS-V4 more intuitively, two fish-hook specimens cut by laser were superimposed on each other. After heating at 180°C for 2 h with the assistance of a small amount of ethylene glycol, they attached to each other and can lift a 2 kg hydrothermal kettle. Lap shear test showed that although the breaking strain after welding decreased, the welded sample still resisted high level of tension (>200 N) (Figure 2c), again demonstrating good

welding capability of TDS-V4. In addition, multiple re-shaping can be designed on TDS-V4 by adjusting the deformation temperature. As illustrated in Figure 2d, different TDS-V4 components were welded into a 3D model of "eagle" (i). Upon heating at 135°C (>T_g) the wings of "eagle" were bent into "V" shape. This temporary deformation was fixed after cooling to room temperature (ii). Once the temperature rose to 135°C again, the temporary "V" wings was completely restored to the original shape (iii). Further heating the wings at 180°C (>T_{mall}) would lead to the formation of permanent "V" shape due to the dynamic bond exchange within TDS-V4 network (iv). This permanent "V" wings also can switch easily among another temporary shape (v), permanent shape (vi), and original shape (i). Obviously, the shape and structural design of TDS-V4 can be achieved by welding and re-shaping at different temperatures, simplifying the manufacturing process and improving the sustainability of materials.

In order to emphasize the dynamic synergistic effect of ester and disulfide bonds on the topological rearrangements of TDS-V4 networks, a control epoxy resin (TES-V4) was designed and synthesized, in which aromatic diamine 4,4'-ethylenedianiline (4-EDL) without disulfide bonds was used as a curing agent instead of 4-DTDA (Figure S8, Supporting Information). As a result, only tertiary amine promoted-ester exchange reaction could occur in this CANs. The curing condition was same as TDS-V4 (Figure S9, Supporting Information), and the cured TES-V4 was transparent and smooth (Figure S10, Supporting Information). Compared with TDS-V4, the TES-V4 had similar T_g of 143°C, v_e of 2561 mol m^{-3}, and better tensile strength of 97 MPa (Figure 2e, S11 and S12, Supporting Information), but much longer relaxation time at a given temperature of 200°C (Figure 2f). Considering the similar T_g and v_e between TDS-V4 and TES-V4, the fast topological rearrangements of TDS-V4 networks was attributed to the synergistic effect of dynamic ester and disulfide bond exchange. Within TDS-V4 networks, ester bonds connected by aromatic disulfide bonds exhibited a considerable rise in mobility and exchange rate due to the breakage of aromatic disulfide bonds and the presence of tertiary amine groups.[15, 39] The improved mobility could lead to faster stress relaxation and network rearrangement of TDS-V4 networks (Figure S13, Supporting Information). On the

contrary, the control of TES-V4 only contained ester bonds, and the lower mobility limited the bond exchange rate within the networks. In short, the good dynamic feature of TDS-V4 together with its high thermal and mechanical properties made it better than most of other reported CANs-tailored resin materials[40-52] (Figure 2g and Table S4, Supporting Information).

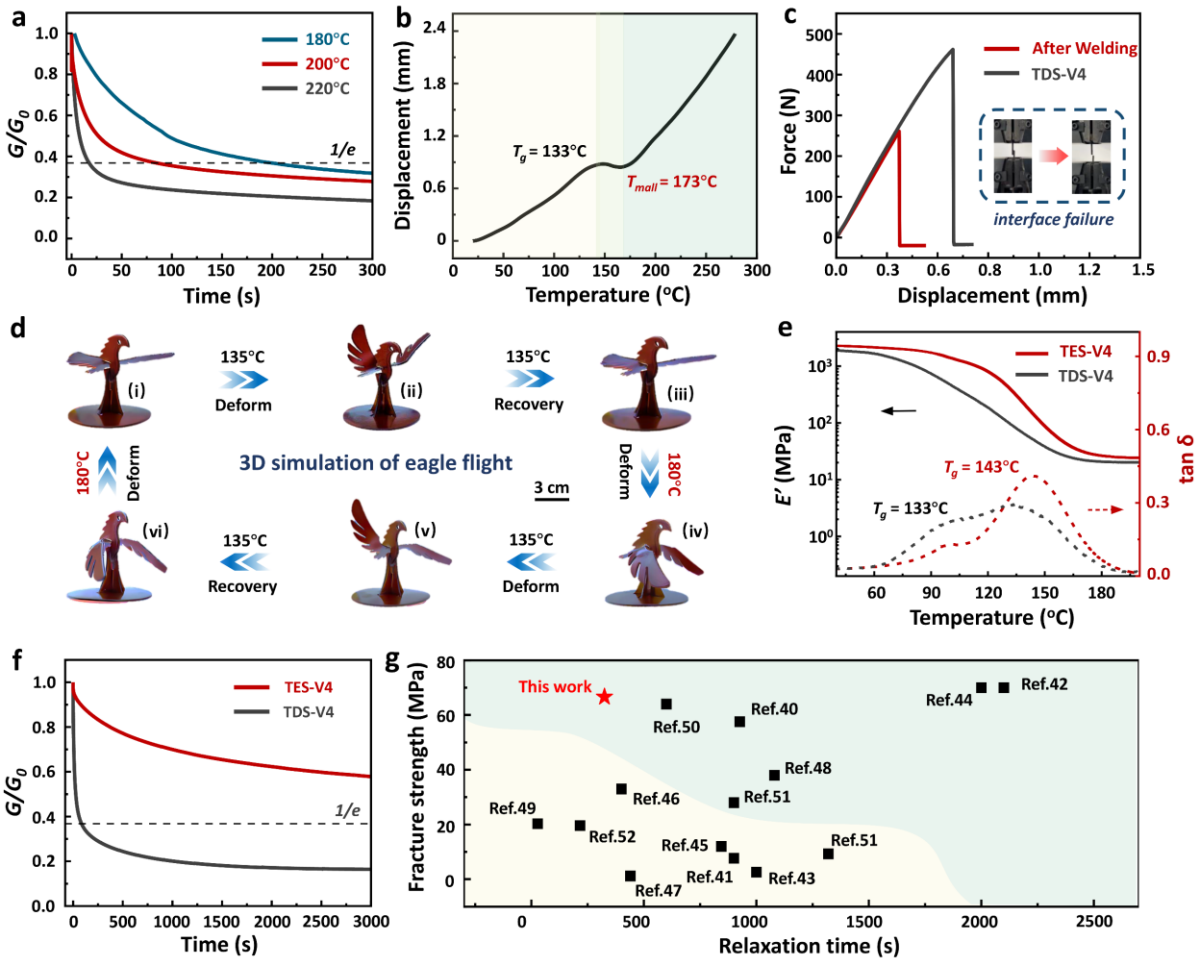

Figure 2. Dynamic network performance. a) Stress relaxation of TDS-V4 in tensile mode at temperatures of 220, 200, and 180°C. b) Thermomechanical analysis of TDS-V4 in the temperature range from 20 to 280°C under a heating rate of 5°C min^{-1}. c) The force displacement curve of TDS-V4 before and after welding at a stretching rate of 2 mm min^{-1}. The welded area was 6 × 5 mm^2. Insert shows the welded sample before and after fracture. d) Digital photos of multiple re-shaping process of the 'eagle flight' made from TDS-V4. e) Storage modulus E' and loss angle tangent tan δ of TDS-V4 and TES-V4 as a function of temperature from -10 to 190°C under a heating rate of 3°C min^{-1}. f) Stress relaxation of TDS-V4 and TES-V4 at 200°C in tensile mode. g) Comparison of T_g, fracture strength, and τ^* at

180°C of TDS-V4 with other reported CANs. Yellow area represents T_g < 60°C while green area represents T_g > 60°C.

2.3 UV-shielding and autonomous visualization of damage and healing

In general, aromatic ring often has UV-shielding ability because of its special electronic and chemical structure. As shown in **Figure 3**a, the transmittance of TDS-V4 network was close to 0% in the range of 200 to 400 nm, demonstrating the blocking power of UV light. It was visually verified in Figure 3b, where the anti-counterfeiting mark on the surface of 100-CNY no longer fluoresced under a 365 nm UV lamp once it was covered by TDS-V4. This UV-shielding ability of TDS-V4 network could be used to prevent UV-induced aging of materials in areas such as aerospace industry and microelectronics packaging.

Autonomous visualization of damage and healing are important in designing safe and intelligent epoxy resins, because it is always difficult to identify the damage and healing at nano/micrometer scale by the naked eye. Figure 3c and S14 (Supporting Information) showed the mechanochromic feature of TDS-V4 network. When the TDS-V4 network was carved or impacted, the damage location immediately turned green, which could be clearly seen by the naked eye. On the contrary, the control of TES-V4 network did not response to mechanical force. Such difference revealed the crucial role of aromatic disulfide bonds in mechanical discoloration behavior. To investigate it in detail, electron paramagnetic resonance (EPR) spectra of the green TDS-V4 powder was studied (Figure 3d). Three anisotropic EPR signals at g_1= 2.0036, g_2= 2.0186, and g_3= 2.0397 were observed clearly, which were attributed to thiyl radicals generated from the cleavage of aromatic disulfide bonds.[53] These radicals, being "frozen" in a polymer network with high T_g, could survive before pairing up to form disulfide bonds again. Its retention duration was quantified by UV-vis spectroscopy in the solid state. As shown in Figure 3e, a peak at 652 nm corresponded to green thiyl radicals. Under high temperature at 180°C, these radicals paired to form disulfide bonds, accompanied with the gradual decrease in absorbance intensity within 4 h, which provided sufficient time for self-reporting the damage in materials.

Moreover, digital and optical microscopy (OM) images of the damage illustrated the healing process of TDS-V4 (Figure 3f and S15, Supporting Information). The width of the scratch on TDS-V4 reduced from 162 μm to almost 0 μm after heating 280 min, and the scratch color gradually returned to reddish brown from the initial green. This healing process can also be monitored quantitatively by converting the RGB value of damage color into the hue value (see Experiment section, Supporting Information). With the extension of heating time, the hue value decreased from 120^{o} to 4^{o}, accompanied with the healing efficiency from 0 to 100%, showing a direct correlation between damage color and healing efficiency (Figure 3g and Table S5, Supporting Information). Apparently, benefiting from the cleavage and the recombination of aromatic disulfide bonds, together with the dynamic ester exchange reaction, TDS-V4 network held potentials to multifunctional engineering materials that required damage self-reporting and healing capabilities.

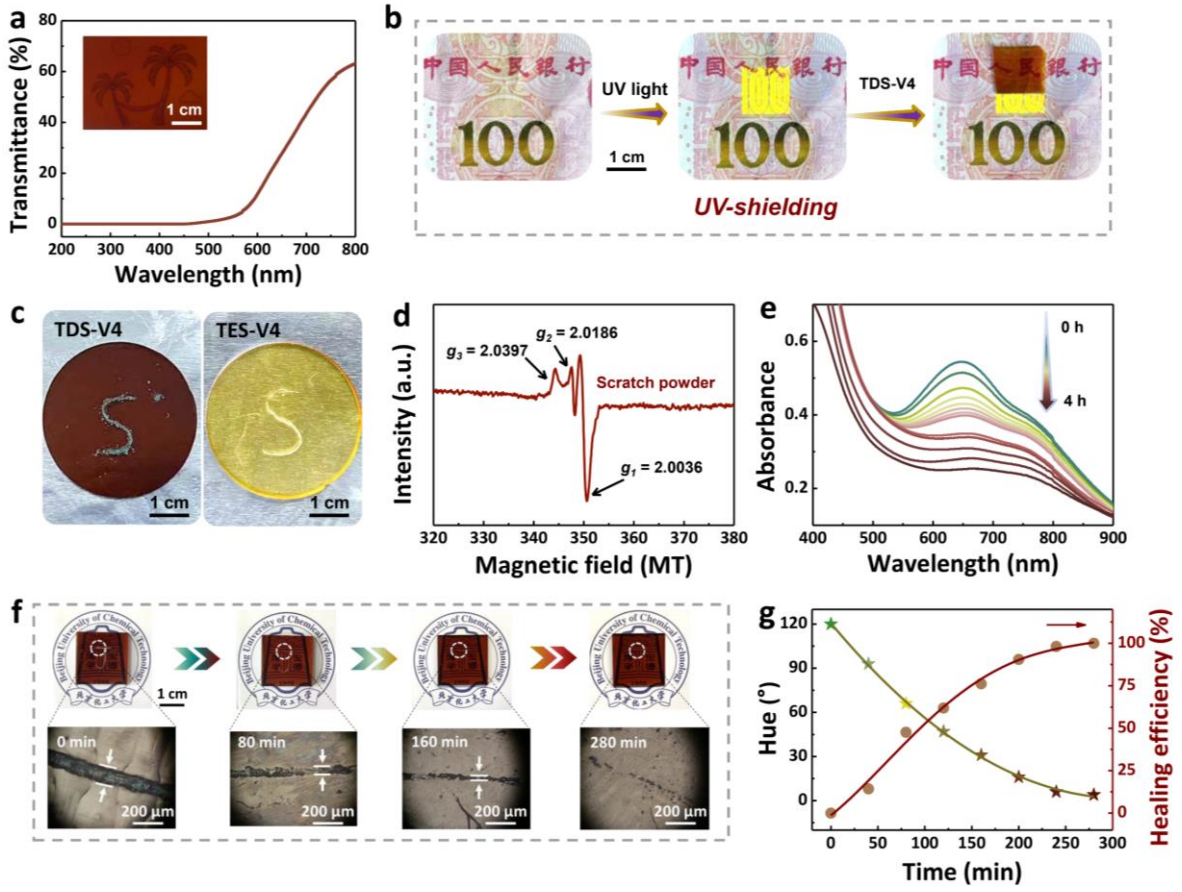

Figure 3. UV-shielding and autonomous visualization of damage and healing. a) Transmission spectrum of TDS-V4 network in the wavelength range of 200-800 nm. Insert is the digital photo

of TDS-V4 film with a thickness of 1.5 mm. b) Digital photos of the security mark covered by TDS-V4 film (thickness of 1 mm) under UV light at 365 nm. c) Mechanochromic behavior of TDS-V4 and TES-V4 upon carving "S" with a knife. d) EPR spectrum of the green powder of TDS-V4 at 25°C. The *g* was calculated according to the equation: hν = *g*βB, where h is Planck's constant, ν is the frequency, β is the Bohr magneton, and B is the magnetic field. e) Time-varying UV-Vis spectra of the green powder of TDS-V4 at 180°C in the range of 400-900 nm. f) Digital photos and optical micrographs of the healing process of TDS-V4 at 180°C. g) Relationship between the hue value of the damage location and healing efficiency during the healing process of TDS-V4.

2.4 Green closed-loop recycling

Chemical recycling of waste epoxy resins in water is appealing, as water is a much greener medium than organic solvents. Due to the presence of tertiary amine-assisted ester bonds, TDS-V4 can be depolymerized in pure water at moderate temperature using hydrothermal reactor (**Figure 4**a). Moreover, the degradation product (DP) would be directly used for resin recovery without the need for separation and purification. Figure 4b showed that no degradation of TDS-V4 networks occurred below 120°C at 10 h, while a dramatic increase in degradation degree (D_d) was observed when the degradation temperature reached 133°C. Noted that the change of D_d closely related to the T_g of TDS-V4. When the temperature was below T_g (<133°C), water molecules were difficult to permeate into the cross-linked network for depolymerization due to the insufficient migration of polymer chain segments.[54] Therefore, when the usage temperature is lower than T_g, the material always has good usage stability. In contrast, once the temperature reached T_g, the cross-linked networks was in rubbery state, and the chain segments had adequate mobility to allow water molecules to effectively swell into the sample, causing the fast cleavage of ester bonds promoted by tertiary amine originated from 4-DTDA (Figure S16, Supporting Information). Under high temperature of 200°C, the D_d can be up to ~53% at 2 h, and a complete degradation of TDS-V4 was achieved within 10 h (Figure 4c). Compared with other degradation process of epoxy resin,[55-60] this degradation method is green, efficient, and pollution-free (Table S6, Supporting Information).

The chemical structure of DP was examined by FTIR (Figure 4d and S17, Supporting Information). Compared with TDS-V4, the DP exhibited remarkable increase in peak intensity at ~3400, 1090, and 1043 cm^{-1} corresponding to -OH groups. The peak associated with C=O group shifted from 1750 to 1720 cm^{-1} after degradation, revealing the generation of carboxyl groups in DP. In addition, the presence of peaks corresponding to aromatic rings (1500 and 1590 cm^{-1}) and ether bond (1168 and 1236 cm^{-1}) indicated that these structures still remained in DP. These results confirmed that most of ester bonds were cleaved in pure water to produce DP in oligomer form with multiple carboxyl and hydroxyl groups. Moreover, the DP can be reused to generate new epoxy resins (rTDS-V4) through an esterification reaction without separation and purification. The DSC curve of the DP showed a significant exothermic peak in the range of 160~190°C, indicative of high curing reactivity of DP. After curing, only glass transition was observed for rTDS-V4, revealing a complete polymerization of DP (Figure 4e). The weakening of hydroxyl peak at 3500 cm^{-1} and the appearance of ester peak at approximately 1720 cm^{-1} in FTIR spectra (Figure 4d), together with the high gel content (Figure S18, Supporting Information), further proved the complete curing of rTDS-V4.

Tensile test showed that rTDS-V4 had high Young's modulus (2.02 GPa), fracture strength (41.3 MPa), and elongation at break (2.48%), the performance recovery of which exceeded 72%, 62% and 80%, respectively (Figure 4f). Compared with TDS-V4, the loss in mechanical properties of rTDS-V4 may be a comprehensive result of the decrease in cross-linking density and material aging. In the degradation process, in addition to the hydrolysis of ester bonds, side reactions such as molecular cleavage were inevitable. Consequently, small molecules generated in side reactions resulted in a decrease in crosslinking density of the re-cured network structure. The DMA results in Figure 4g confirmed our hypothesis that the T_g of rTDS-V4 decreased from the original 133°C to 91°C, while the ν_e of rTDS-V4 reduced from 2292 to 1591 mol/m^3, much lower than that of TDS-V4. In addition, the recycled rTDS-V4 still had good reshaping processability (Figure 4h). In terms of depolymerization and repolymerization, our TDS-V4 network had the following advantages in comparison with other recyclable epoxy resin:[13, 60-65] (1) Green and simple. Water was a green reaction medium, and the DP can be

directly obtained without complex separation and purification process. (2) Zero emissions. No gas was generated during the degradation process. (3) Circular economy. The whole process did not require the doping of other petrochemical raw materials, effectively reducing the cost and the use of chemical resources.

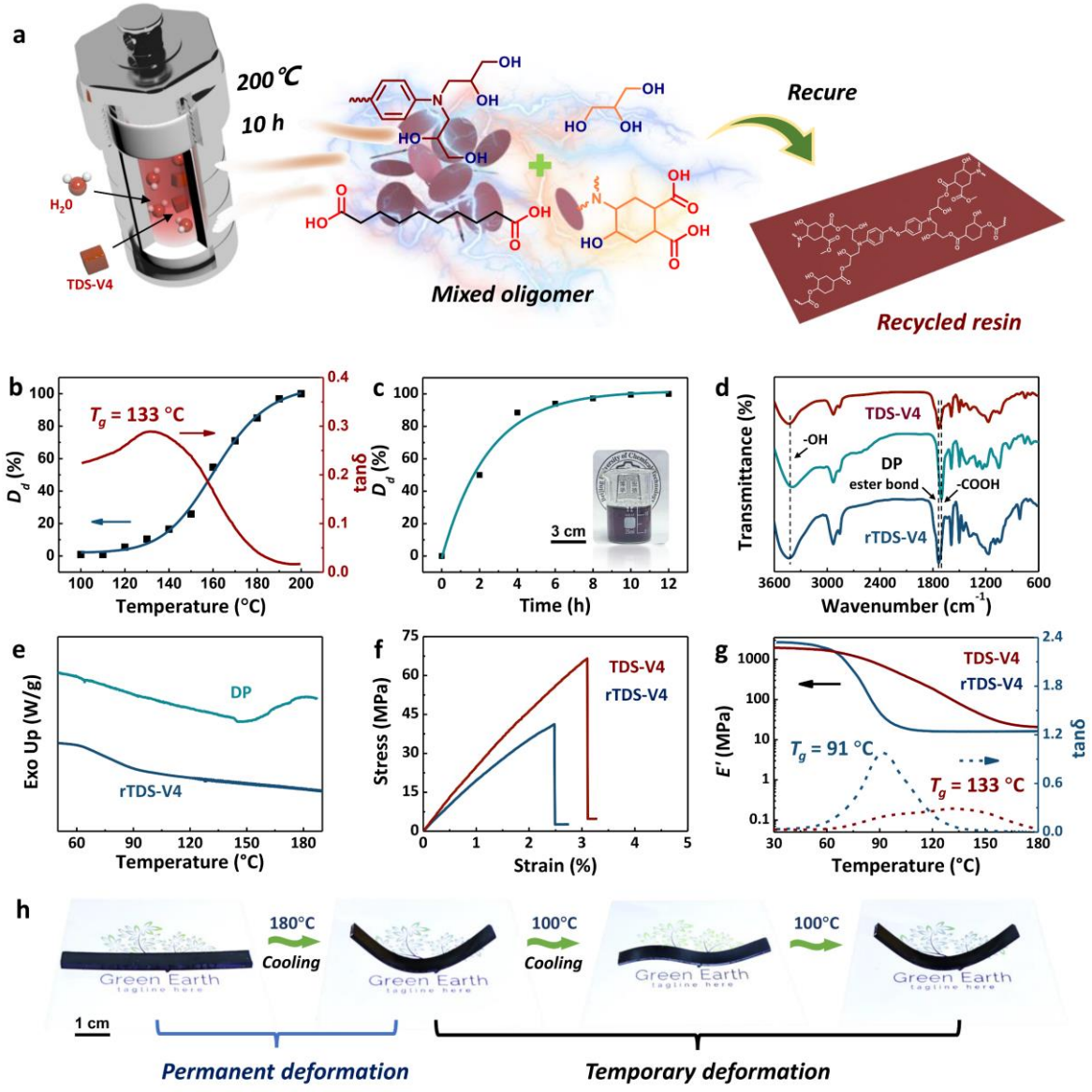

Figure 4. Green closed-loop recovery. a) Procedure diagram of pure water-mediated closed-loop recovery. b) The effect of temperature on degradation degree (D_d) of TDS-V4 within the temperature range of 100-200°C at 10 h. c) The degradation kinetics of TDS-V4 at 200°C in pure water. Insert is digital photo of aqueous solution of TDS-V4 after complete degradation. d) FTIR spectra of TDS-V4, DP, and rTDS-V4 in the wavenumber range from 3600-600 cm^{-1}.

e) DSC curves of DP before and after curing from 50 to 190°C at a heating rate of 5 and 10°C min^{-1}, respectively. f) Tensile stress-strain curves of TDS-V4 and rTDS-V4 at a stretching rate of 2 mm min^{-1}. g) Storage modulus E' and loss angle tangent tan δ as a function of temperature from 30 to 180°C under a heating rate of 3°C min^{-1}. h) Digital photos of multiple re-shaping process of rTDS-V4.

3. Conclusion

In summary, we have prepared mechanically robust epoxy resins (TDS) implementing dynamic ester and disulfide bonds. The TDS exhibited superior mechanical properties (tensile strength and tensile modulus of 66.6 MPa and 2.63 GPa, flexural strength and flexural modulus of 103.2 MPa and 3.52 GPa) and high glass transition temperature (133°C). Due to the presence of disulfide bonds and tertiary amine-assisted ester bonds, TDS owned good welding and re-shaping ability. Moreover, the reversible transformation between aromatic disulfide bonds and thiyl radicals endowed TDS with mechanochromic property for autonomous visualization of damage and healing. More interestingly, TDS can be completely degraded in pure water using hydrothermal reactor through tertiary amine-assisted depolymerization. The degradation product could be further recycled to produce new epoxy resins without complex purification process and additional raw materials. This work provides a simple and economical strategy for the development of high-performance, versatile, renewable cutting-edge resins.

Statistical Analysis

All data were obtained from at least three independent samples and expressed as the mean ± standard deviation (n = 3 for polymer characterization and mechanical studies).

Supporting Information

Supporting Information is available from the Wiley Online Library or from the author.

Acknowledgements

This work is supported by Beijing Natural Science Foundation (L233016).

Conflict of Interest

The authors declare no conflict of interest.

Data Availability Statement

Research data are not shared.

Received: ((will be filled in by the editorial staff))
Revised: ((will be filled in by the editorial staff))
Published online: ((will be filled in by the editorial staff))

References

[1] F. Vidal, E. R. van der Marel, R. W. F. Kerr, C. McElroy, N. Schroeder, C. Mitchell, G. Rosetto, T. T. D. Chen, R. M. Bailey, C. Hepburn, C. Redgwell, C. K. Williams, *Nature* **2024**, *626*, 45.

[2] L. Dai, R. Ruan, S. You, H. Lei, *Science* **2022**, *337*, 934.

[3] P. Shieh, W. Zhang, K. E. L. Husted, S. L. Kristufek, B. Xiong, D. J. Lundberg, J. Lem, D. Veysset, Y. Sun, K. A. Nelson, D. L. Plata, J. A. Johnson, *Nature* **2020**, *583*, 542.

[4] Y. Jiang, J. Li, D. Li, Y. Ma, S. Zhou, Y. Wang, D. Zhang, *Chem. Soc. Rev.* **2024**, *53*, 624.

[5] A. Ahrens, A. Bonde, H. Sun, N. K. Wittig, H. C. D. Hammershøj, G. M. F. Batista, A. Sommerfeldt, S. Frølich, H. Birkedal, T. Skrydstrup, *Nature* **2023**, *617*, 730.

[6] Y. Wen, C. Chen, Y. Ye, Z. Xue, H. Liu, X. Zhou, Y. Zhang, D. Li, X. Xie, Y. Mai, *Adv. Mater.* **2022**, *34*, 2201023.

[7] A. Sudheshwar, N. Malinverno, R. Hischier, B. Nowack, C. Som, *Resour. Conserv. Recycl.* **2023**, *189*, 106757.

[8] J. Wan, B. Gan, C. Li, J. Molina-Aldareguia, E. N. Kalali, X. Wang, D. Wang, *Chem. Eng. J.* **2016**, *284*, 1080.

[9] Y. Huang, Y. Zhou, X. Zeng, D. Zhang, S. Wu, *Adv. Mater.* **2023**, *35*, 2305517.

[10] J. H. Shin, M. B. Yi, T. H. Lee, H. J. Kim, *Adv. Funct. Mater.* **2022**, *32*, 2207329.

[11] J. Peng, S. Xie, T. Liu, D. Wang, R. Ou, C. Guo, Q. Wang, Z. Liu, *Compos. Part B-Eng.* **2022**, *242*, 110109.

[12] Y. Zhang, H. Yan, R. Yu, J. Yuan, K. Yang, R. Liu, Y. He, W. Feng, W. Tian, *Adv. Sci.* **2023**, *11*, 2306350.

[13] M. Chen, W. Luo, S. Lin, B. Zheng, H. Zhang, *Compos. Part B-Eng.* **2023**, *257*, 110666.

[14] L. Gao, W. Jia, F. Shi, H. Huo, D. Zhou, H. Liu, B. Zhang, *Acta Mater. Compos. Sin.* **2023**, *40*, 2587.

[15] C. Cui, F. Wang, X. Chen, T. Xu, Z. Li, K. Chen, Y. Guo, Y. Cheng, Z. Ge, Y. Zhang, *Adv. Funct. Mater.* **2024**, DOI: 10.1002/adfm.202315469.

[16] Y. Shen, B. Wang, D. Li, W. Yuan, Y. Huang, Z. Hu, *Chem. Eng. J.* **2023**, *455*, 140889.

[17] R. Karasik, N. E. Lauer, A. E. Baker, N. E. Lisi, J. A. Somarelli, W. C. Eward, K. Fürst, M. M. Dunphy-Daly, *Front. Mar. Sci.* **2023**, *9*, 1017247.

[18] E. Topham, D. McMillan, S. Bradley, E. Hart, *Energy Policy* **2019**, *129*, 698.

[19] A. M. Wemyss, C. Bowen, C. Plesse, C. Vancaeyzeele, G. T. M. Nguyen, F. Vidal, C. Wan, *Mat. Sci. Eng. R* **2020**, *141*, 100561.

[20] W. Zou, J. Dong, Y. Luo, Q. Zhao, T. Xie, *Adv. Mater.* **2017**, *29*, 1606100.

[21] Z. Zhang, D. Lei, C. Zhang, Z. Wang, Y. Jin, W. Zhang, X. Liu, J. Sun, *Adv. Mater.* **2023**, *35*, 2208619.

[22] T. Habets, G. Seychal, M. Caliari, J. M. Raquez, H. Sardon, B. Grignard, C. Detrembleur, *J. Am. Chem. Soc.* **2023**, *145*, 25450.

[23] J. Cui, F. Liu, Z. Lu, S. Feng, C. Liang, Y. Sun, J. Cui, B. Zhang, *Adv. Mater.* **2023**, *35*, 2211417.

[24] G. Seychal, L. Van Renterghem, C. Ocando, L. Bonnaud, J. M. Raquez, *Compos. Part B-Eng.* **2024**, *272*, 111201.

[25] Q. Chang, W. Li, L. Xiao, K. Zhang, J. Huang, Y. Wang, X. Nie, J. Chen, *Macromol. Chem. Phys.* **2023**, *224*, 2300272.

[26] B. Zhang, T. Cui, X. Jiao, Y. Ma, L. Gao, J. Hu, *Chem. Eng. J.* **2023**, *476*, 146625.

[27] J. Han, T. Liu, C. Hao, S. Zhang, B. Guo, J. Zhang, *Macromolecules* **2018**, *51*, 6789.

[28] J. L. Self, C. S. Sample, A. E. Levi, K. Li, R. Xie, J. R. de Alaniz, C. M. Bates, *J. Am. Chem. Soc*. **2020,** *142*, 7567.

[29] D. Reisinger, M. U. Kriehuber, M. Bender, D. Bautista-Anguís, B. Rieger, S. Schlögl, *Adv. Mater.* **2023**, *35*, 2300830.

[30] M. Delahaye, J. M. Winne, F. E. Du Prez, *J. Am. Chem. Soc.* **2019**, *141*, 15277.

[31] F. Van Lijsebetten, J. O. Holloway, J. M. Winne, F. E. Du Prez, *Chem. Soc. Rev.* **2020**, *49*, 8425.

[32] J. Zhao, Z. Zhang, C. Wang, X. Yan, *CCS Chem.* **2024**, *6*, 41.

[33] W. Yang, Y. Zhu, T. Liu, D. Puglia, J. M. Kenny, P. Xu, R. Zhang, P. Ma, *Adv. Funct. Mater.* **2023**, *33*, 2213294.

[34] C. Shi, D. He, B. Wang, Q. Zhang, H. Tian, D. Qu, *Angew. Chem. Int. Ed.* **2022**, *62*, e202214422.

[35] A. R. de Luzuriaga, J. M. Matxain, F. Ruipérez, R. Martin, J. M. Asua, G. Cabañero, I. Odriozola, *J. Mater. Chem. C* **2016**, *4*, 6220.

[36] F. Dénès, M. Pichowicz, G. Povie, P. Renaud, *Chem. Rev.* **2014**, *114*, 2587.

[37] N. Teng, J. Dai, S. Wang, J. Hu, X. Liu, *Chem. Eng. J.* **2022**, *428*, 131226.

[38] M. Ge, G. Liang, A. Gu, *Chem. Eng. J.* **2023**, *475*, 146269.

[39] X. Xu, S. Ma, H. Feng, J. Qiu, S. Wang, Z. Yu, J. Zhu, *Polym. Chem.* **2021**, *12*, 5217.

[40] Y. Xu, S. Dai, H. Zhang, L. Bi, J. Jiang, Y. Chen, *ACS Sustainable Chem. Eng.* **2021**, *9*, 16281.

[41] Y. Liu, J. He, Y. Li, X. Zhao, J. Zeng, *Compos. Commun.* **2020**, *22*, 100445.

[42] Y. Liu, S. Ma, Q. Li, S. Wang, K. Huang, X. Xu, B. Wang, J. Zhu, *Eur. Polym. J.* **2020**, *135*, 109881.

[43] D. Berne, F. Cuminet, S. Lemouzy, C. Joly-Duhamel, R. Poli, S. Caillol, E. Leclerc, V. Ladmiral, *Macromolecules* **2022**, *55*, 1669.

[44] Y. Liu, Z. Yu, B. Wang, X. Xu, H. Feng, P. Li, J. Zhu, S. Ma, *Eur. Polym. J.* **2022**, *173*, 111272.

[45] S. Mu, Y. Zhang, J. Zhou, B. Wang, Z. Wang, *ACS Sustainable Chem. Eng.* **2020**, *8*, 5296.

[46] S. Debnath, S. Kaushal, U. Ojha, *ACS Appl. Polym. Mater.* **2020**, *2*, 1006.

[47] X. Yan, T. Liu, C. Hao, L. Shao, Y. Chang, Z. Cai, S. Shang, Z. Song, J. Zhang, *Ind. Crops Prod.* **2023**, *202*, 116976.

[48] J. Li, S. Zhang, B. Ju, *J. Appl. Polym. Sci.* **2022**, *139*, e52676.

[49] J. Chen, Y. Zhang, Y. Wang, L. Chen, *Polymer* **2023**, *281*, 126083.

[50] J. Liu, K. V. Bernaerts, *Chem. Eng. J.* **2023**, *477*, 147299.

[51] J. Lu, Z. Li, J. Chen, S. Li, J. He, S. Gu, B. Liu, L. Chen, Y. Wang, *Research* **2022**, *2022*, 9846940.

[52] X. Huang, Y. Wang, C. Ding, S. Zhang, X. Duan, H. Ji, J. Cai, Z. Wang, *ACS Appl. Polym. Mater.* **2024**, *6*, 126.

[53] Y. Amamoto, H. Otsuka, A. Takahara, K. Matyjaszewski, *Adv. Mater.* **2012**, *24*, 3975.

[54] T. Liu, L. Shao, B. Zhang, Y. Chang, J. Zhang, *Macromol. Rapid Commun.* **2022**, *43*, 2200538.

[55] J. Yang, J. Liu, W. Liu, J. Wang, T. Tang, *J. Anal. Appl. Pyrol.* **2015**, *112*, 253.

[56] W. Dang, M. Kubouchi, H. Sembokuya, K. Tsuda, *Polymer* **2005**, *46*, 1905.

[57] J. Zhu, P. Chen, M. Su, C. Pei, F. Xing, *Green Chem.* **2019**, *21*, 1635.

[58] B. Zhang, T. Cui, X. Jiao, Y. Ma, L. Gao, J. Hu, *Chem. Eng. J.* **2023**, *476*, 146625.

[59] Y. Wang, X. Cui, H. Ge, Y. Yang, Y. Wang, J. Li, T. Deng, Z. Qin, X. Hou, *ACS Sustain. Chem. Eng.* **2015,** *3*, 3332.

[60] H. U. Sokoli, M. E. Simonsen, R. P. Nielsen, J. Henriksen, M. L. Madsen, N. H. Pedersen, E. G. Søgaard, *Ind. Eng. Chem. Res*. **2016**, *55*, 9118.

[61] K. Yu, Q. Shi, M. L. Dunn, T. Wang, H. J. Qi, *Adv. Funct. Mater.* **2016**, *26*, 6098.

[62] A. Ghorai, H. Chung, *Adv. Funct. Mater.* **2024**, DOI: 10.1002/adfm.202403035.

[63] H. Si, L. Zhou, Y. Wu, L. Song, M. Kang, X. Zhao, M. Chen, *Compos. Part B-Eng.* **2020**, *199*, 108278.

[64] L. Anderson, E. W. Sanders, M. G. Unthank, *Mater. Horiz.* **2023**, *10*, 889.

[65] Y. Deng, Q. Zhang, D. H. Qu, H. Tian, B. L. Feringa, *Angew. Chem. Int. Ed.* **2022**, *61*, e202209100.